Nanoscale

Accepted Manuscript

This article can be cited before page numbers have been issued, to do this please use: O. Seivert, I. Janica, B. Mukherjee, C. Corcelle, S. Eigler, P. Samorì, S. Garaj and A. Bianco, *Nanoscale*, 2026, DOI: 10.1039/D6NR01024E.

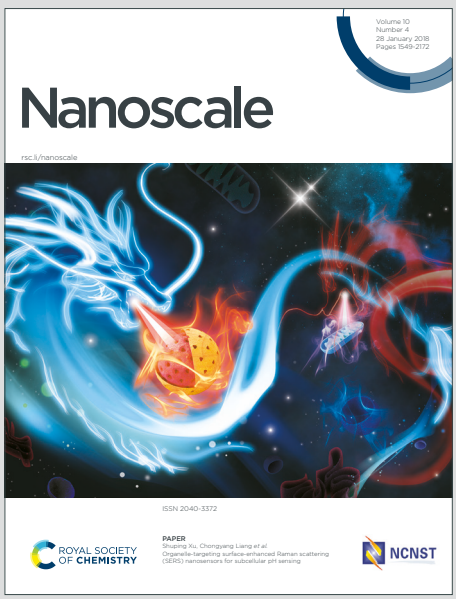

ROYAL SOCIETY OF CHEMISTRY

rsc.li/nanoscale

View Article Online
DOI: 10.1039/D6NR01024E

ARTICLE

Reactivity and mechanistic insights into multistep silane functionalization of oxo-graphene

Received 00th January 20xx,
Accepted 00th January 20xx

DOI: 10.1039/x0xx00000x

Océane Seivert,[a] Iwona Janica,[b] Bristy Mukherjee,[c] Céline Corcelle,[a] Siegfried Eigler,[d] Paolo Samorì,[b] Slaven Garaj,[c] Alberto Bianco[a,*]

oxo-Graphene (oxoG), an alternative form of graphene oxide with a low number of defects, is regarded as a versatile platform for covalent surface modification due to its abundant oxygen functional groups and large surface area. Among the different functionalization strategies, the epoxide ring opening is widely employed. However, reactions using bifunctional molecules like 3-aminopropyltriethoxysilane (APTES) often produce unpredictable outcomes, jeopardizing the characterization and hampering a clear identification of the chemical structure of the resulting conjugate. Here, we investigate the functionalization of oxoG with APTES in different solvents, providing unequivocal evidence that the amine group preferentially reacts via the epoxide ring opening. The resulting oxoG-APTES was characterized by X-ray photoelectron spectroscopy, and thermogravimetric analysis. Subsequent silanization with (3-glycidyloxypropyl)trimethoxysilane (GPTMS) confirmed the presence of terminal silane groups, and further nucleophilic ring-opening with 4-(trifluoromethyl)benzylamine (FMBA) validated the stepwise covalent modification. Simplified molecular model reactions analyzed by ^{1}H NMR corroborated these findings and highlighted the critical influence of solvent and temperature on the outcomes of multistep reactions. This study provides a detailed mechanistic understanding of oxoG functionalization using silanes and demonstrates the importance of combining complementary analytical techniques to unambiguously characterize the different conjugates, enabling more predictable design of graphene-based nanomaterials for advanced applications.

Introduction

Among carbon-based materials, graphene is a widely recognized two-dimensional carbon nanomaterial. Its unique structure confers to graphene numerous interesting properties including a high surface area, excellent thermal[1,2] and electrical conductivity,[3–5] high mechanical properties[6] and chemical stability.[7] However, despite these advantages, pristine graphene possesses poor colloidal stability in aqueous media due to its hydrophobicity, strong π-π stacking interactions and poor degree of functionalization promoting aggregation, limiting its dispersibility and consequently limiting its use.[8]

Graphene oxide (GO) is one of the oxidized derivatives of graphene obtained by oxidizing graphite in strong acid conditions.[9] It exhibits better dispersibility in water and in polar solvents due to the enriched GO surface with a variety of oxygen functional groups such as hydroxyls, epoxides, carboxyl and carbonyl groups at defect sites or rims of flakes. Additionally, GO retains the large specific area of graphene,[10] and part of the π-structure of pristine graphene, permitting its easy functionalization via covalent,[11–13] and non-covalent approaches[13] (e.g., via π-π stacking and H-bonds). In the past 10 years, milder oxidation conditions have been proposed to synthesize another type of GO corresponding to oxo-graphene (oxoG). Compared to GO, oxoG can be considered as defect-free, with a still high amount of oxygenated groups, as its size and surface chemistry can be precisely controlled during the synthesis.[14] Epoxides and hydroxyl groups are the most abundant functional groups present on the basal planes of GO and oxoG, whereas carboxyl and carbonyl functions are confined mainly to their edges and represent less than 3.5% of functions.[15] As a result, most covalent functionalization of these two nanomaterials are carried out on epoxides and hydroxyl groups. Due to their ring strain, the epoxides exhibit high reactivity and are easily opened by nucleophilic attack. Among various nucleophiles, amines have been widely employed for the functionalization of GO or oxoG through epoxide ring opening, without requiring additional activating or coupling agents.[15]

However, when bifunctional (or multifunctional) molecules are used, the functionalization of GO and oxoG often becomes less predictable and the determination of the chemical structure of the obtained conjugates is challenging. This issue is more pronounced when the molecules used possess two or more reactive groups, as each of them may independently react with GO, potentially leading to competitive or simultaneous reactions. This complexity complicates the identification of the predominant reaction and prevents a clear characterization of the structure of the resulting materials.

[a] CNRS, Immunology, Immunopathology and Therapeutic Chemistry, UPR 3572, University of Strasbourg, ISIS, 8 Allée Gaspard Monge, 67000 Strasbourg, France; E-mail: a.bianco@ibmc-cnrs.unistra.fr
[b] Université de Strasbourg and CNRS, ISIS and icFRC, 8 Allée Gaspard Monge, 67000 Strasbourg, France
[c] Department of Physics, Department of Biomedical Engineering and Department of Materials Science and Engineering, National University of Singapore, Singapore, Singapore
[d] Institute of Chemistry and Biochemistry, Freie Universität Berlin, Takustrabe 3, 14195, Berlin, Germany

View Article Online
DOI: 10.1039/D6NR01024E

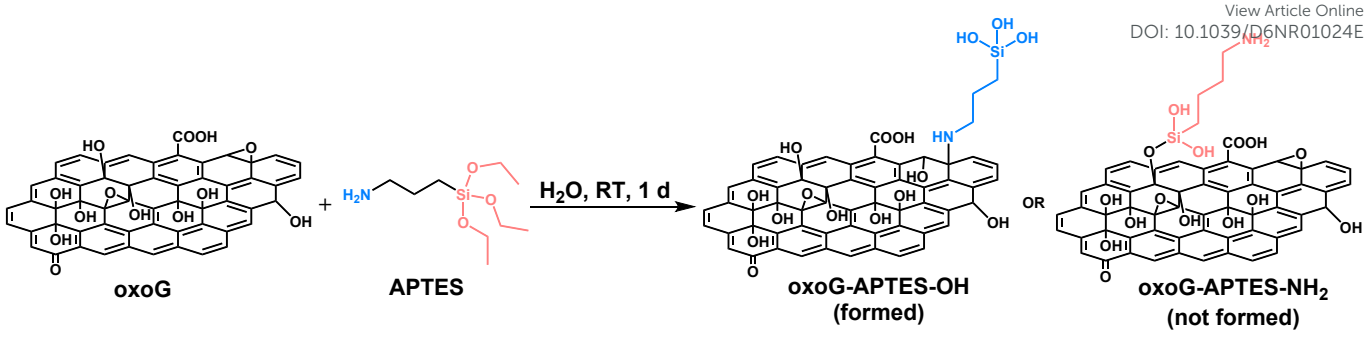

Scheme 1. Chemical reactions of APTES on oxoG via its amino group or its siloxane group, leading to oxoG-APTES-OH and oxoG-APTES-NH_2, respectively. Note: the epoxides are generally localized at the basal plane of GO. One epoxide is kept at the edge for better clarity in illustrating the ring opening reaction.

A key example is represented by the covalent functionalization of GO with 3-aminopropyltriethoxysilane (APTES), either involving the reaction of the ethoxysilane moiety of APTES with the hydroxy or carboxy groups of GO forming C-O-Si bonds[16–25], or involving the amine function of APTES reacting by ring epoxide opening creating C-NH-C secondary amino group[22–30]. Depending on the reaction conditions, different reactivities and products were described in the literature[21,30] leading to some confusing and inconclusive evidences on the actual generated conjugates. This is even more troublesome if further modifications are envisaged. In most cases, functionalization was conducted in organic solvents, at high temperatures, with long reaction times, allowing the formation of a covalent bond between GO and APTES. However, these conditions usually promote hydrolysis of APTES and subsequently self-condensation and cross-linking, encapsulating the nanomaterial into a thick silicon-based polymeric layer. To better investigate the reactivity of APTES, we have decided to use oxoG, another form of oxidized graphene similar to GO.[14] Additionally, the reaction was performed at room temperature in order to attempt to minimize the self-condensation of APTES and the encapsulating of oxoG.

Based on these considerations, herein, we describe a multistep modification of oxoG using silane molecules. oxoG was firstly functionalized with APTES in aqueous solution at room temperature. A silanization reaction of oxoG-APTES with 3-glycidyloxypropyl)trimethoxysilane (GPTMS) was subsequently performed to prove the reactivity of silanol groups of APTES and indirectly the initial reaction of APTES on oxoG through its amine moiety. Finally, the opening of the terminal epoxide of GPTMS with a nucleophile was conducted to further prove the reaction of oxoG-APTES with GPTMS through silanization and the presence of terminal epoxides of GPTMS. Each reaction step was characterized using a combination of X-ray photoelectron spectroscopy (XPS) and thermogravimetric analysis (TGA). To confirm the multistep reactions on oxoG, the entire process was repeated on simplified small organic models and each step was analyzed using NMR.

Results and discussion

The multifunctionalization of GO and oxoG has gained a lot of interest for the development of new composites and catalysts, as well as for application in biosensing and drug delivery.[31,32] Various coupling reagents such as silanes, amines, thiols, and carbodiimides have been used to introduce functional groups aiming to enhance dispersibility and chemical versatility. Among these, APTES functionalization of GO has been widely reported,[31–34] though inconsistent results raise questions about its reactivity. In this study, to investigate the reactivity of APTES, we decided to use oxoG.[33].

The functionalization of oxoG to obtain oxoG-APTES was performed by reacting an excess of APTES with a solution of oxoG in distilled water, at room temperature, for 1 day (**Scheme 1**). As reported in the literature, the reaction of APTES on oxoG can occur following two ways: 1) the amine moiety can react by ring epoxide opening, leading to the formation of oxoG-APTES-OH, and 2) the siloxane moiety can react with the hydroxyl or carboxyl groups leading to the formation of oxoG-APTES-NH_2 (**Scheme 1**). Under aqueous conditions, the hydrolysis of the ethoxy groups of APTES occurs, generating silanol groups and promoting this dual reactivity on oxoG. After the reaction, the resulting conjugate was centrifuged and washed 3 times with deionized water (DI) to remove the unreacted APTES. The resulting conjugate was then analyzed by XPS (**Figure S1**). The survey spectrum of oxoG-APTES revealed the presence of 67.2% of C, 25.8% of O, 3.1% of N and 3.9% of Si. The silicon-to-nitrogen ratio is approximately 1:1, consistent with the atomic composition of APTES, which contains one nitrogen atom and one silicon atom. The high-resolution C 1s spectrum was deconvolved into six peaks at 283.15 eV (C-Si), 284.73 eV (C-C/C=C), 285.50 eV (C-N), 286.62 eV (C-O), 287.51 eV (C=O), and 288.66 eV (COOH/π-π* satellite). The high-resolution O 1s spectrum indicates the presence of C-Si-O/Si-O-Si bond at 532.41 eV, while the high-resolution Si 2p spectrum (**Figure 1A**) shows three main peaks at 101.97 eV (C-Si-O), 102.67 eV (O-Si-O) and 103.88 eV (Si-O-Si). The high-resolution N 1s spectrum of oxoG-APTES indicates the presence of three contributions at 399.42 eV (R-NH2), 400.41 eV (R-NH-R) and 401.59 eV (R-NH_3^+) (**Figure S1**). The presence of the secondary amine confirms the covalent grafting of APTES onto oxoG. Additionally, the presence of the primary amine suggests that APTES polymerize during the reaction.

View Article Online
DOI: 10.1039/D6NR01024E

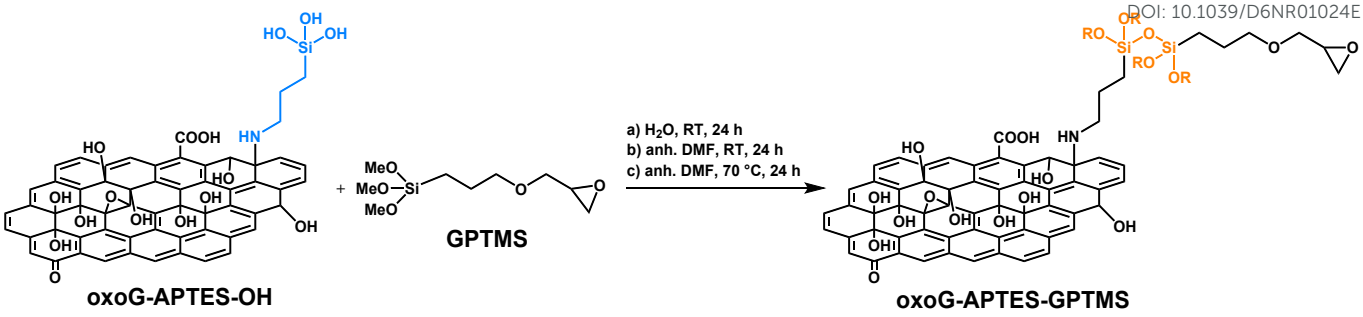

Scheme 2. Silanization reaction of oxoG-APTES-OH with GPTMS using three different experimental conditions. R corresponds to substituents derived from hydrolyzed and/or partially condensed silane species.

These results confirm the presence of APTES bound to oxoG. Overall, these observations are consistent with the literature, although they do not permit to unambiguously determine which functional group of APTES reacted preferentially on oxoG. It is important to mention that the use of bifunctional coupling agents may, in principle, lead to inter-sheet cross-linking in graphene oxide-based materials.[35,36] Following hydrolysis, alkoxysilane groups can undergo condensation reactions to form siloxane (Si–O–Si) networks, which may bridge adjacent sheets if reactive surface groups are present simultaneously.[37] In addition, the primary amine functionality of APTES may react with epoxide groups located on neighbouring oxoG sheets via nucleophilic ring-opening reactions, potentially resulting in covalent inter-sheet connections.[38] Such competing grafting, cross-linking and self-condensation processes depend strongly on the density of reactive groups and the reaction conditions."

To identify which functional group of APTES preferentially reacted on oxoG, two hypotheses were made: 1) if the amine group reacts via ring epoxide opening, a terminal silanol would remain available at the surface (oxoG-APTES-OH) (**Scheme 1**). This silanol could subsequently undergo condensation with another siloxane; and 2) if the siloxane group reacts with the hydroxyl function of oxoG, a terminal amine would be present at the surface (oxoG-APTES-NH_2) (**Scheme 1**). This amine could be further used as functional group and react with other molecules. To verify these two hypotheses, a bifunctional molecule bearing both a silane and an electrophilic site is required. GPTMS is a suitable candidate due to its dual functionality comprising a trialkoxysilane group at one end capable of undergoing condensation reactions with Si-OH groups of APTES, and an epoxide ring at the other end, which can participate in a nucleophilic addition. The reaction between oxoG-APTES and GPTMS was performed using three different experimental conditions, based on the hypothesis that GTPMS reacts on oxoG-APTES-OH primarily through its siloxane moiety (**Scheme 2**), *i.e.*: a) reaction in DI water at RT, b) reaction in anhydrous (anh). DMF at RT, and c) reaction in anh. DMF at 70 °C, all for 24 h. The aqueous condition was chosen as water catalyzes the hydrolysis of GPTMS, thereby enhancing its reactivity with oxoG-APTES through silanol formation and subsequent condensation. The hydrolysis of GPTMS followed by its condensation was already described in the literature, but the reactions were performed using specific conditions (*e.g.*, acidic or basic pH).[39,40] In contrast, the use of anhydrous DMF conditions was employed to assess the role of water in the reactivity of GPTMS. In absence or in low amount of water, the effect of temperature on the reactivity of GPTMS was also explored. A reaction temperature of 70 °C was chosen considering the presence of methoxy groups on GPTMS. This temperature would facilitate methanol elimination, thereby promoting a subsequent more efficient condensation reaction with oxoG-APTES.

The conjugated materials resulting from each condition were analyzed using XPS (**Figure 1** and **Figures S2-S4**). Compared to the initial oxoG-APTES material, the surveys revealed an increase of silicon content of 3.4% in oxoG-APTES-GPTMS in H2O at RT, no changes in oxoG-APTES-GPTMS in anh. DMF at RT and an increase of 0.5% in oxoG-APTES-GPTMS in anh. DMF at 70 °C (Table S1 in SI). These results indicate that in anh. DMF at RT, GPTMS did not react on oxoG-APTES, as evidenced by the absence of a clear increase in the silicon content, relative to the starting oxoG-APTES material. The presence of water appears to be necessary for the reaction to proceed efficiently at RT. In contrast, conducting the reaction in anh. DMF at 70 °C resulted in a measurable increase in silicon content, indicating that elevated temperature promotes GPTMS attachment even in the absence of water molecules.".

View Article Online
DOI: 10.1039/D6NR01024E

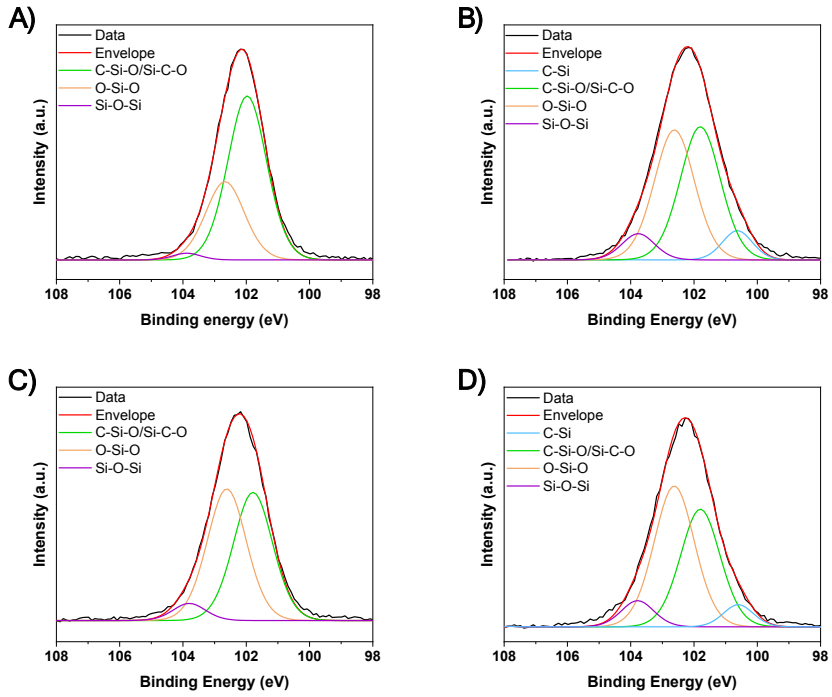

Figure 1. High-resolution Si 2p spectra of A) oxoG-APTES, B) oxoG-APTES-GTPMS (H_2O, RT, 24 h), C) oxoG-APTES-GTPMS (anh. DMF, RT, 24 h), D) oxoG-APTES-GTPMS (anh. DMF, 70 °C, 24 h)

Additionally, the high-resolution Si 2p spectra show for the three conditions an increase of the O-Si-O deconvoluted bond (102.60 eV) and Si-O-Si (103.88 eV) compared to oxoG-APTES (**Figure 1**). The increased intensity of the Si-O-Si and O-Si-O deconvoluted bonds has to be interpreted, as it may result from a combination of self-polymerization of GPTMS and condensation reaction with oxoG-APTES. Indeed, in these experiments, 2.2 mg of oxoG-APTES were reacted under the three GPTMS conditions considered. Regarding, the reaction performed in aqueous conditions, approximately 3 mg were isolated. In contrast, the reactions performed in anh. DMF yielded 2.2 mg at RT and 2.3 mg at 70 °C. The higher mass obtained for oxoG-APTES-GPTMS (H_2O, RT, 24 h) indicates that GTPMS exhibits increased reactivity under aqueous conditions, likely through self-polymerization and/or condensation with oxoG-APTES. Regarding the high-resolution O 1s spectra, no changes were observed between oxoG-APTES and the three conditions tested to form oxoG-APTES-GPTMS, as observed from the four peaks at 530.34 eV (C-O), 531.60 eV (C=O), 532.41 eV (C-Si-O/Si-O-Si) and 533.87 eV (OH/COOH) displaying similar intensities.

Overall, the reaction between GPTMS and oxoG-APTES have occurred more efficiently in DI water at RT, followed by the reaction in anh. DMF at 70 °C, while no reaction was observed for the conditions in anh. DMF at RT.

Subsequently, TGA was performed for oxoG, oxoG-APTES, and the three oxoG-APTES-GPTMS samples prepared under the different conditions (**Figure S5**). The TGA curve of pristine oxoG exhibits the typical two-step thermal degradation profile. The first weight loss of approximately 40% around 200 °C was attributed to the thermal decomposition of the labile surface C-OH functional groups and epoxy-groups.[41] The second weight loss of around 10% between 200 and 300 °C, was associated with the thermal decomposition of bounded organosulfate groups, which originates from the sulfuric acid used during the synthesis of oxoG, which did not fully hydrolyze during the work-up at low temperatures.[42,43]

The TGA profile of oxoG-APTES is consistent with the literature, exhibiting four main thermal degradation steps.[22,44] At 200 °C, the reduced weight loss of approximately 20% was significantly lower than the pristine oxoG and was attributed to the desorption of adsorbed water as well as the consumption of C-O epoxy functional groups of oxoG during the reaction with APTES. This result corroborates the covalent grafting of APTES at the surface of oxoG. At higher temperatures, a similar weight loss of about 20% between 300 and 550 °C was observed, suggesting thermal decomposition of organic moieties introduced by APTES, including cleavage of Si–C bonds and degradation of oxygen and nitrogen-containing groups.[45]

In the case of oxoG-APTES-GPTMS samples synthesized in DMF, both materials display similar TGA profiles. A major weight loss of approximately 50-55% between 150 and 200 °C is observed, which could originate from the release of labile groups within the material structure. A second gradual weight loss of 15-20% between 200 and 400 °C likely corresponds to thermal decomposition of C-O functional group of GPTMS, as well as the decomposition of oxygen and nitrogen moieties of APTES molecule, similar to the degradation observed for oxoG-APTES. Finally, a third weight loss was observed between 400 and 800 °C. In contrast, oxoG-APTES-GPTMS synthesized in aqueous solution displays a reduced weight loss at 200 °C (~10%).

View Article Online
DOI: 10.1039/D6NR01024E

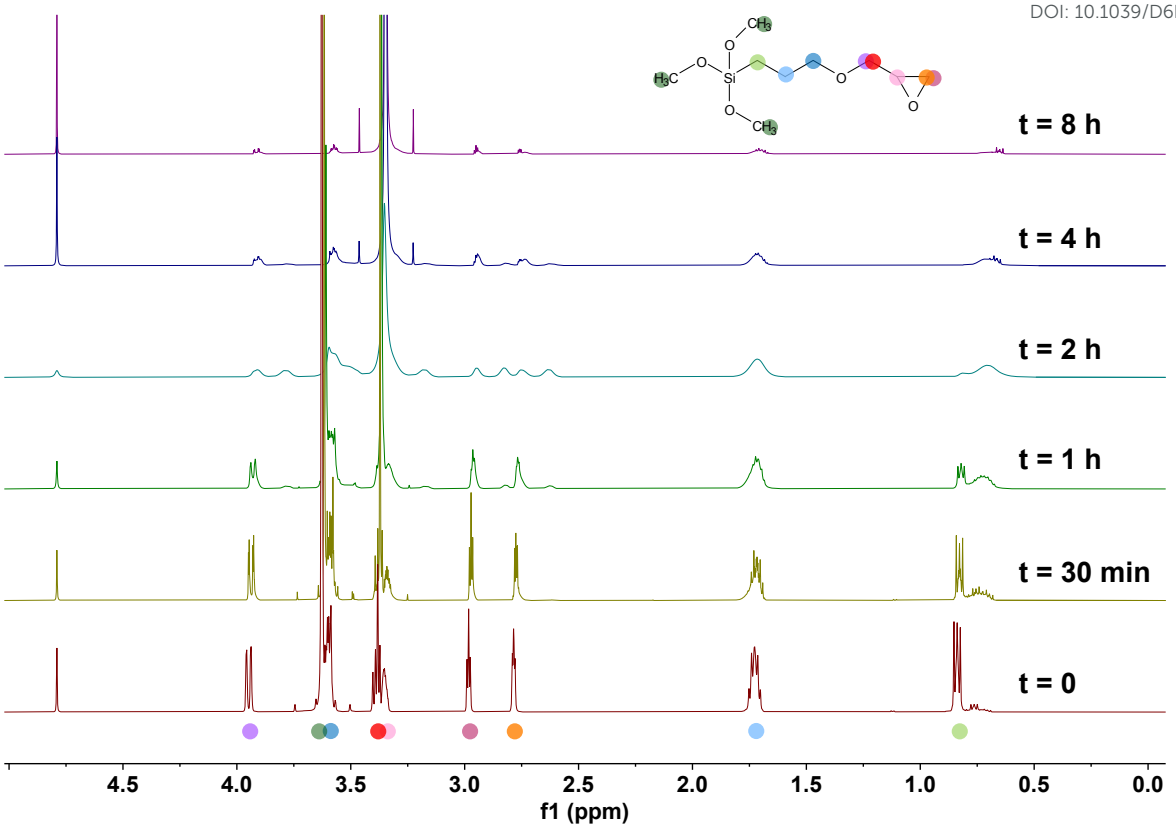

Figure 2. ^{1}H NMR spectra of GPTMS in D_2O at t = 0, 30 min, 1, 2, 4 and 8 h.

At 350 °C, an additional 15% weight loss is observed, followed by a major weight loss between 350 and 600 °C (~30%). This degradation is likely associated with the degradation of the organosilane moieties which might indicate the presence of a high degree of functionalization of the APTES moiety. Similarly to the result obtained by XPS, the thermogravimetric analysis suggests that the reaction between oxoG-APTES and GPTMS performed in aqueous media provides efficient functionalization.

To understand the behavior of GPTMS under different reaction conditions, it is important to consider its tendency for hydrolysis and self-condensation. Silane coupling agents, such as GPTMS, are known to undergo hydrolysis in the presence of water, which can lead to oligomerization or polymerization even before reacting with other substrates. For these reasons, for the reaction in aqueous solution, we considered the possibility that GPTMS can undergo hydrolysis and subsequent self-polymerization prior of reacting with oxoG-APTES, resulting in the formation of a polysiloxane polymer that remains after the purification.[46] To assess this hypothesis, a control reaction was performed in which GPTMS was exposed to aqueous and anhydrous DMF conditions using model compounds. The polymerization kinetics of GPTMS in water and anhydrous DMF were studied using ^{1}H NMR in deuterated solvents (*i.e.*, D_2O and DMF-d_7). Briefly, the ^{1}H NMR spectra of each condition were recorded at RT at 0, 30 min, 1, 2, 4, and 8 h. A final spectrum was recorded after 24 h in DMF-d_7. Regarding the DMF-d_7, the water content was below 0.05%, ensuring nearly anhydrous conditions. To maintain this condition and obtain reliable results, all experiments in DMF-d_7 were conducted in screwed-cap NMR tubes to prevent moisture from the air to enter during the reaction. The samples were prepared using preconditioned needles and the reagent additions were carried out rapidly to minimize exposure to atmospheric moisture. The chemical shift of H_2O in DMF-d_7 was reported at 3.50 ppm. Due to proper handling of the anhydrous conditions, the presence of water in the obtained NMR spectra was negligeable.

The polymerization kinetics of GPTMS in D_2O evidenced a decrease of the concentration of GPTMS over time, as the intensity of each peak diminished in comparison to the H_2O residual signal used as standard (**Figure 2**). After 30 min, the peak at 3.63 ppm related to the methoxy group on the silane (dark green) is slightly shifted to 3.62 ppm and a peak at 3.37 ppm start appearing, indicating the hydrolysis of GPTMS. The peaks at 3.62 and 3.37 ppm are further shifted at 3.60 and 3.30 ppm, respectively, and after 2 h signals of the methoxy group disappeared. This process clearly led to the formation of methanol as a consequence of the hydrolysis of GPTMS. After half an hour, a new peak appears at 0.73 ppm, indicating a change in the local environment of the proton in green, originally at 0.83 ppm as depicted in **Figure 2**.

View Article Online
DOI: 10.1039/D6NR01024E

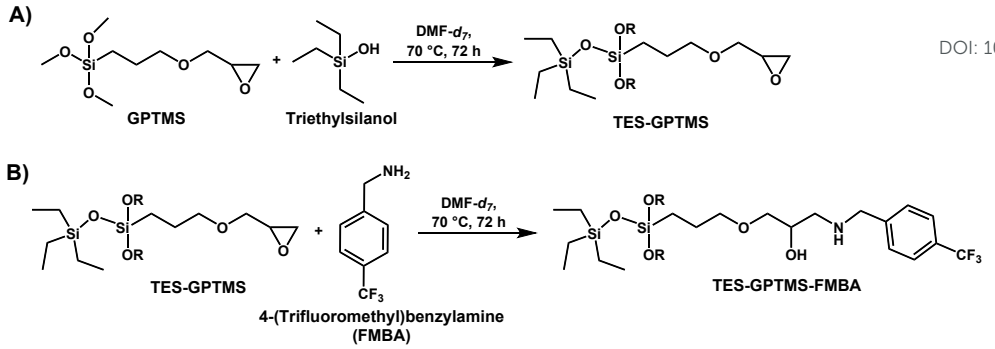

Scheme 3. Schematic representation of the reaction between A) GPTMS and TES and B) TES-GPTMS and FMB

Over time, all peaks broaden, and new peaks at 2.83 and 2.63 ppm appear confirming the progression of the polymerization.[46]

After 4 h, a white precipitate is observed at the bottom of the NMR tube showing the formation of a polymer, which is insoluble in D_2O. Contrary to what was reported in literature, in our case, the hydrolysis and condensation of GPTMS did not require the use of acidic or basic condensation. In contrast, GPTMS is stable in deuterated DMF at RT as no changes of the intensity or shape of the signals were detected up to 24 h (**Figure S6**).

Accounting for the polymerization kinetics of GPTMS observed in D_2O, the reaction between oxoG-APTES and GPTMS was further analyzed by XPS for reaction times of 30 min, 1 h, and 2 h (**Figure S7-S9**). The XPS survey revealed that no reaction occurred after 30 min, whereas a small increase of silicon content compared to the nitrogen content was observed after 2 h. This increase was comparable to that observed for the reaction performed in DMF at 70 °C. However, the high-resolution N 1s spectra of each reaction time did not show the presence of any secondary amine deconvoluted peak, indicating that the grafting of APTES does not occur at short reaction time (**Figure S7-S9**). Additionally, these results indicate that the polymerization of APTES is the first process occurring before the covalent grafting to the material.

Since the NMR analysis confirmed that GPTMS undergoes rapid hydrolysis followed by self-polymerization in aqueous solution, whereas it remains chemically stable under anhydrous DMF, these data imply that the results previously obtained by XPS need to be considered carefully. The reaction of oxoG-APTES with GPTMS in H_2O might lead to the highest silicon increase as a result of a partial self-polymerization and a partial condensation with oxoG-APTES. This observation is further supported by the insolubility of the resulting polymer in water, as evidenced in the NMR tube, which prevents its removal during the purification by centrifugation. These findings underscore the importance of carefully considering solvent choice during silanization reactions, as it can significantly influence the outcome and potentially lead to misinterpretation of the results. Thus, we decided to perform the following reactions and analyses with the oxoG-APTES-GPTMS conjugate obtained in anh. DMF at 70 °C to avoid issues caused by decomposition reactions.

As a promising result was also obtained for oxoG-APTES-GPTMS prepared in anhydrous DMF at 70 °C, it was decided to acquire greater insight into the addition of GPTMS to oxoG-APTES under this condition. Towards this end, we designed a simple reaction using a model compound (**Scheme 3A**) and followed this reaction by ^{1}H NMR. TES-OH (triethylsilanol) was selected to mimic the oxoG-APTES system with a single hydroxyl group and three alkyl chains to avoid the formation of multiple products (**Scheme 3A**). The TES-GPTMS conjugate was analyzed by ^{1}H NMR every 24 h to monitor the progress of the reaction. The spectra were compared with those of the individual GPTMS and TES-OH molecules, recorded under identical concentration and temperature conditions. After 72 h, the reaction was stopped, (**Figure 3A**), assuming that TES-OH and GPTMS underwent silanization condensation, the protons adjacent to the silicon atoms in both molecules were expected to exhibit chemical shift variations relative to those of the individual species in deuterated DMF. In GPTMS, the protons of the signals of interest in the alpha carbon (green) and beta carbon (blue) of the silicon moiety (**Figure S10**) were observed at 0.66 and 1.63 ppm, while those of TES-OH, i.e., the protons of the signals in the alpha carbon (turquoise) and beta carbon (fuchsia) of the silicon moiety (**Figure S11**) appeared at 0.52 and 0.95 ppm respectively.

The ^{1}H NMR spectrum of TES-GPTMS revealed distinct chemical shift changes compared to the spectra of the individual reactants. Specifically, for the GPTMS moiety, the signal of the protons originally observed at 0.66 ppm (proton in green) shifted to 0.73 ppm, and the signal at 1.63 ppm (proton in blue) shifted to 1.71 ppm (**Figure 3A and S10**). In the case of the TES moiety, the protons at 0.52 ppm (proton in turquoise) were shifted to 0.63 ppm, while the signal at 0.95 ppm (proton in fuchsia) shifted to 1.00 ppm (**Figure 3A and S11**). Additionally, the disappearance of the methoxy group signal at 3.55 ppm of GPTMS, accompanied by the appearance of a new singlet at 3.50 ppm, assigned to methanol, confirmed the release or thermal elimination/cleavage of the methoxy groups of GPTMS, leading to condensation.

View Article Online
DOI: 10.1039/D6NR01024E

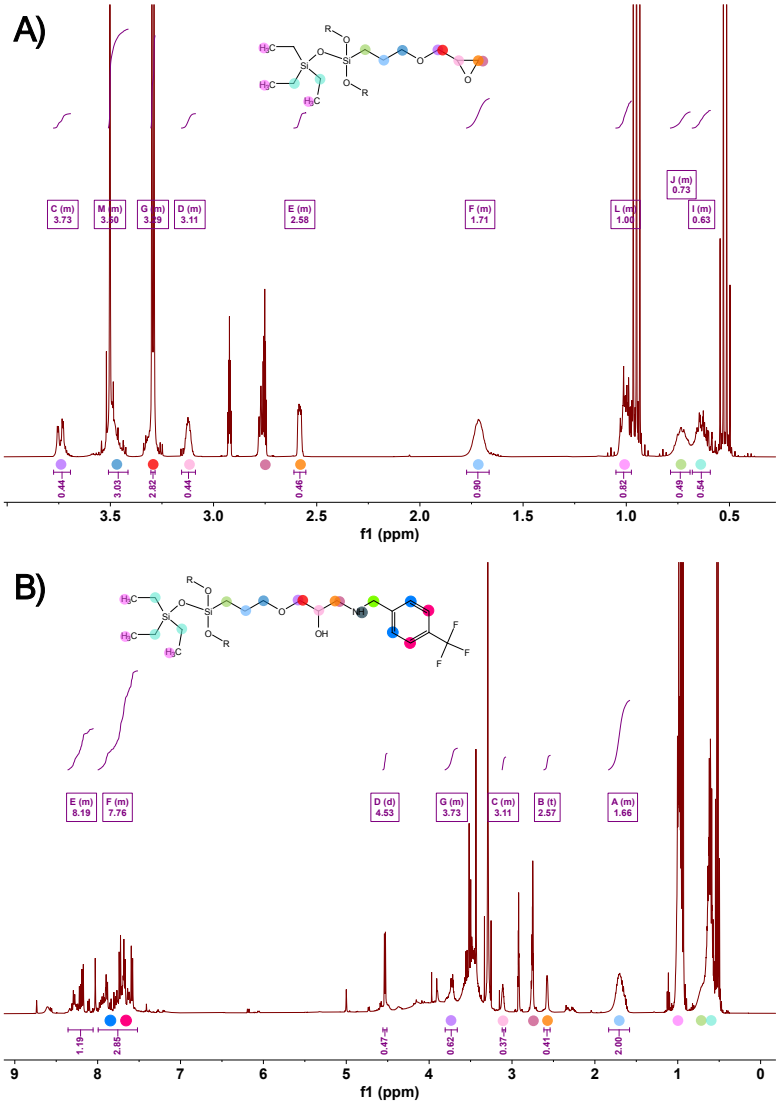

Figure 3. 1H NMR spectra of A) TES-GPTMS and B) TES-GPTMS-FMBA in DMF-*d7* after reaction for 72 h at 70 °C.

However, the presence of residual signals of the TES group indicates an incomplete conversion (25%), while a fraction of GPTMS likely underwent self-polymerization. This was confirmed by the broadening of the other GTPMS proton signals. It should be noted that this self-polymerization can occur in all reactions, although the degree of polymerization might vary between each experiment.

Nonetheless, the presence of at least one accessible hydroxyl group per GPTMS molecule enabled the formation of the expected product (TES-GPTMS). This result allowed us to confirm the occurrence of the reaction of GPTMS with oxoG-APTES, as assessed by XPS analysis of oxoG-APTES-GPTMS in anhydrous DMF at 70 °C. Additionally, these results underscore the importance of carefully selecting appropriate solvents and reaction conditions when multiple steps are performed on graphene-based materials. Our study reveals that the interpretation of data obtained by XPS and TGA should be analyzed with care before drawing definitive conclusions on the obtained conjugates.

As we were able to obtain and characterize the desired conjugate, namely oxoG-APTES-GPTMS, we decided to prove the reactivity of the available epoxide at the end of the silane moiety. To this aim, the terminal epoxide of GPTMS was involved in a nucleophilic ring opening reaction with an amino compound. 4-Trifluoromethyl-benzylamine (FMBA) was chosen as target nucleophile to form oxoG-APTES-GPTMS-FMBA (**Scheme 4**). The presence of the CF_3 group facilitates the identification of the product by XPS, as it can be observed by the appearance of a distinct F 1s peak in the survey spectrum shown in **Figure S12**, corresponding to 2.0% in agreement with the atomic content of the other elements. The high-resolution deconvoluted XPS F 1s spectrum displays one peak at 688.21 corresponding to -CF_3 binding energy. The high-resolution deconvoluted C 1s spectrum further confirmed the presence of fluorine by the C-F peak at 292.38 eV. The TGA profile of oxoG-

View Article Online
DOI: 10.1039/D6NR01024E

APTES-GPTMS-FMBA presented a three-step thermal degradation (**Figure S5**).

View Article Online
DOI: 10.1039/D6NR01024E

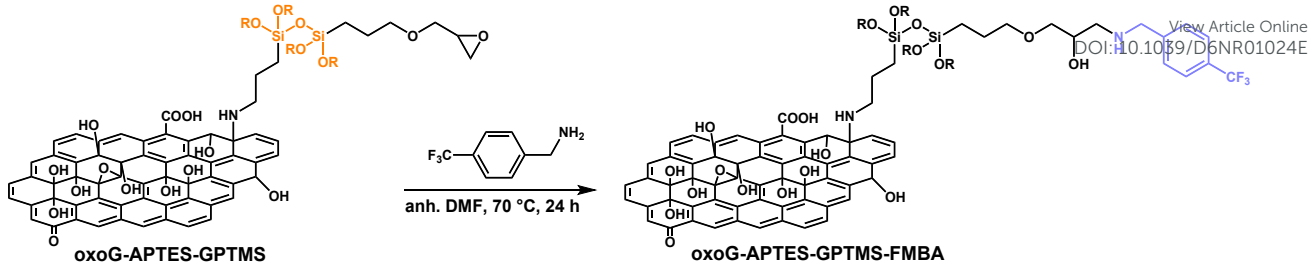

Scheme 4. Schematic representation of the reaction between FMBA and oxoG-APTES-GTPMS (anh. DMF, 70 °C, 24 h).

The first degradation step of approximately 10% weight loss between 130 and 210 °C, is likely attributed to the desorption of residual DMF solvent used during the synthesis. The second step degradation between 210 and 440 °C, corresponding to a 20% weight loss, is attributed to the thermal degradation of residual C-O groups, similarly to oxoG-APTES and oxoG-APTES-GPTMS (anh. DMF, 70 °C).

A final weight loss of 30% is observed between 440 and 490 °C. At higher temperatures, the material remains relatively stable. The differences observed compared to the TGA profile of oxoG-APTES-GPTMS (anh. DMF, 70 °C) suggest that a covalent reaction has occurred between oxoG-APTES-GPTMS and FMBA. As previously demonstrated, oxoG was successfully functionalized with APTES, followed by a silanization step which was confirmed by the increase in the silicon content. Finally, the epoxide moiety of GPTMS was opened using FMBA as a nucleophile.

To validate the occurrence of the epoxide ring opening, we followed the reaction using again a simple multistep process and studied the products by ^{1}H NMR. For this purpose, TES-GPTMS was reacted with one equivalent of FMBA in the NMR tube (**Scheme 3B**). The mixture was then heated at 70 °C for 4 days and the spectrum of the resulting mixture was recorded every 24 h at RT in DMF-d_7 (**Figure 3B**). For comparison, the ^{1}H NMR spectrum of FMBA in DMF-d_7 was recorded, focusing on the possible shift of the protons of the amine (indicated by dashed grey in the chemical structure of **Figure S13**) and of the methylene group of the benzylamine derivative (dashed green in **Figure S13**). Concerning the GPTMS moiety, the protons of interest were instead those of the epoxide ring, located at 3.11 ppm (pink), 2.75 ppm and 2.58 ppm (orange), with the signal at 2.75 ppm overlapping with the residual signal of deuterated DMF (**Figure S10**). The ^{1}H NMR of TES-GPTMS-FMBA analysis revealed no chemical shift for any of these protons. However, a noticeable decrease in the intensity of the peak at 3.90 ppm, corresponding to the proton of the methylene group of FMBA, was observed. Surprisingly, a new doublet appeared at 4.53 ppm and additional peaks are observed in the aromatic region at a slightly lower field compared to the molecule of FMBA alone. To better understand if the reaction was providing the hypothesized compound, we further analyzed the mixture by 2D NMR. The doublet at 4.53 ppm in the HSQC spectrum is assigned to a CH_2 proton (carbon at 40.86 ppm) (**Figure S14**). HMBC correlations indicate three neighboring carbons at 128.31 ppm, 144.56 ppm, and 161.51 ppm (**Figure S15A and S15B**). The carbon at 144.56 ppm shows no proton correlation in the HSQC spectrum, consistent with a quaternary carbon (**Figure S16**). The carbon at 128.31 ppm correlates with a proton in the aromatic region (red spot in HSQC), suggesting it is a CH (or a CH_3) (**Figure S18**). The carbon at 161.51 ppm also shows correlations in the aromatic region, but overlaps with the DMF residual solvent peak, making the assignment uncertain (**Figure S17**). Based on these correlations, the doublet at 4.53 ppm corresponds to the proton indicated in dashed green in **Figure 3B**. The neighboring carbon observed in HMBC spectrum at 128.31 ppm can be assigned to the dashed blue carbon, while the quaternary carbon at 144.56 ppm can be linked to the adjacent aromatic carbon of FMBA. Overall, these results indicate that the doublet at 4.53 ppm arise from the FMBA molecule and appears after FMBA undergoes the reaction. The HSQC and HMBC correlations are consistent with the appearance of additional peaks in the aromatic region, indicating a change of environment for the molecule of FMBA. This supports the statement that FMBA reacted with the epoxide group of GPTMS on TES-GPTMS. The reactions between TES-OH and GTPMS and then TES-GPTMS and FMBA were repeated three times, each time giving similar results, and indicating that FMBA reacts with GPTMS through nucleophilic epoxide ring opening. Finally, to confirm the result on the simple molecular system, a deuterated analogue of FMBA was synthesized. The idea behind this synthesis was to obtain a structural analogue of FMBA containing deuterium atoms in the carbon alpha to the nitrogen and in the amine function. The corresponding non-deuterated benzylamine analogue was also employed as control. If the doublet observed at 4.53 in the case of TES-GPTMS-FMBA derive from the FMBA molecule resulting from its reaction with the epoxide of GPTMS, the substitution of the hydrogen with deuterium should eliminate this coupling signal in the NMR spectrum. Moreover, since the benzylamine is a stronger nucleophile compared to FMBA, the reaction with GPTMS was expected to proceed in a more efficient way. For this purpose, phenylmethan-d_2-amine-d_2 (benzylamine-d_4, **Figure S19**) was prepared from benzonitrile and $LiAlD_4$ and benzylamine (**Figure S20**) was used as a secondary proof of reaction.

As in the previous experiments, the reaction between TES-GPTMS and either benzylamine or benzylamine-d_4 was performed at 70 °C in DMF-d_7 for 4 days and the ^{1}H NMR, HSQC and HMBC spectra were recorded (**Figure 4, Figure S21**).

View Article Online
DOI: 10.1039/D6NR01024E

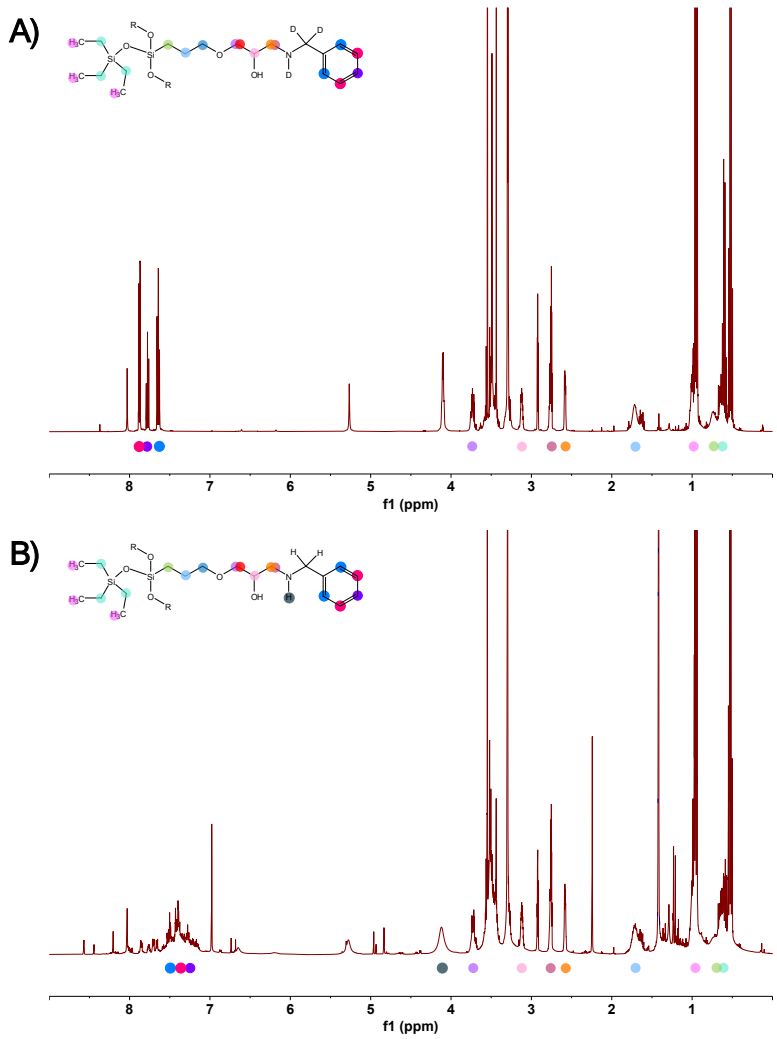

Figure 4. ^{1}H NMR spectra of A) TES-GPTMS-benzylamine-d_4 and B) TES-GPTMS-benzylamine in DMF-d_7

In the case of TES-GPTMS-benzylamine-d_4 (**Figure 4A**) the ^{1}H NMR was simpler compared to TES-GPTMS-FMBA, consistent with the disappearance of the proton-proton coupling pattern of the aromatic ring. Indeed, the previous observed doublet at 4.53 ppm was no longer detected.

When compared to its non-deuterated analogue TES-GPTMS-benzylamine (**Figure 4B**), the appearance of additional peaks in the aromatic region provides the first evidence of the reaction occurrence. This suggests that the environment of the benzyl ring changed upon reaction. No doublet at 4.53 ppm was observed but a new doublet at 4.83 ppm and a broad singlet at 4.12 ppm appeared, the latter arising from the N-H group following epoxide opening.

In the HSQC spectrum (**Figure S21**), the 4.83 ppm doublet correlated with a CH_2 carbon, while the HMBC spectrum (**Figure S22A and S22B**) revealed three neighboring carbons at 128.21, 140.27, and 162.13 ppm, similarly to the pattern observed for TES-GTPMS-FMBA. The carbon at 128.21 ppm (**Figure S25**) correlated with a proton in the aromatic region, whereas the carbon at 140.27 ppm (**Figure S23**) showed no proton correlation, indicating a quaternary carbon. The carbon at 162.13 ppm (**Figure S24**) overlaps with the DMF residual solvent peak, making the assignment uncertain. This spectral pattern was similar to TES-GTPMS-FMBA, but was absent in TES-GPTMS-benzylamine-d_4, confirming that the doublet at 4.53 ppm (in the case of TES-GPTMS-FMBA) and at 4.83 ppm (in the case of TES-GPTMS-benzylamine) originate from the proton at the alpha-carbon next to the amine function, appearing upon ring epoxide opening of GPTMS.

These experiments unambiguously confirmed that nucleophilic molecule can indeed react with TES-GPTMS, providing indirect evidence that the epoxide of the GPTMS moiety remains stable after formation of the TES-GPTMS conjugate. This further demonstrates that GPTMS reacts with TES-OH through silanization. Consequently, these results reveal that FMBA reacted with oxoG-APTES-GPTMS through epoxide ring opening and proved that multistep reactions can be conducted under controlled reaction conditions, leading to complex silane functionalized graphene-based materials.
Although the observed changes in elemental composition provide clear evidence for the successive functionalization

View Article Online
DOI: 10.1039/D5NR01024E

steps, a reliable determination of an absolute grafting density turned out being extremely challenging. Due to the carbon-rich nature of both oxoG and the grafted silane species, no invariant substrate signal is available for straightforward quantification by XPS. Likewise, the overlapping decomposition processes of the carbon framework and the residual silane-derived species observed by TGA prevent an unambiguous estimation of the amount of grafted species.

Finally, the insights gained here provide a foundation for the rational design of multifunctional graphene derivatives with controlled surface chemistry.

Experimental Section

Materials and methods

All chemicals used in the experiments were obtained from commercial sources as analytical reagents and were used as received. oxoG was prepared in the laboratory of Prof. Siegfried Eigler, and fully described and characterized in our previous work (corresponding to oxo-G1).[33] 3-Aminopropyltriethoxysilane, (3-glycidyloxypropyl)trimethoxysilane and 4-trifluoromethyl-benzylamine were purchased from Sigma-Aldrich. Anhydrous DMF (anh. DMF), anhydrous THF (anh. THF), triethylsilanol and $LiAlH_4$ were obtained from Thermo Scientific. Deuterated water and deuterated DMF (DMF-d_7) were purchased from Eurisotop. $LiAlD_4$ was obtained from Janssen Chimica and benzonitrile was obtained from Fluka AG.

^1H, ^{13}C, ^1H-^{13}C HSQC and ^1H-^{13}C HMBC NMR spectra were recorded on Bruker AV500 300 instrument operating at 500 MHz for ^1H NMR and 125 MHz for ^{13}C NMR. Tetramethylsilane or residual solvents were used as internal reference. The peak values were obtained as ppm (δ) and calibrated to the references. The resonance multiplicity is indicated as s (singlet), d (doublet), t (triplet), dd (doublet of doublet), and m (multiplet). X-ray photoelectron spectroscopy was conducted by a multiprobe system (Thermo Scientific) equipped with an Al Kα source (1486 eV) at pressure of 10^{-8}-10^{-9} mbar in the main chamber. The X-ray spot size was settled at 400 µm. Survey spectra were recorded as result of 20 scans with a pass energy of 200.00 eV and a step size of 1 eV, while the high-resolution spectra were an average of at least 30 scans with a pass energy of 50.00 eV and a step size of 0.1 eV. All spectra were charge-corrected by referencing the C-C/C=C component of the C 1s spectrum to 284.8 eV and fitted using Thermo Scientific Avantage software after Smart background subtraction. Peak assignments were based on literature values[47] and equivalent chemical environments were constrained to similar binding energies across all samples. Furthermore, the FWHM of equivalent components was kept constant whenever possible and only minimally adjusted when required to obtain physically meaningful fits and facilitate quantitative comparison. Tables containing fitted peak positions, peak areas and relative atomic percentages are available in the Supporting Information (Table S2 and S3). The samples were prepared by filtering 0.5 mL of solution through a 0.1 µm PTFE membrane, air-dried, and transferred onto copper tape by direct adhesion. Thermogravimetric analyses were performed by using a TGA Q500 TA instrument 3 with a heating rate of 10 °C·min^{-1} from room temperature to 800 °C under N_2 with a flow rate of 50 mL·min^{-1} using aluminium pans. Centrifugation was performed on an Eppendorf centrifuge 5804 R at 5000 rpm and at 4 °C for 15 min.

2. Synthesis and characterization of the different oxoG conjugates and the model molecules

2.1. oxoG-APTES. oxoG (8.33 mL) at an initial concentration of 3.6 mg mL^{-1} was dispersed in 21.67 mL of distilled (DI) water leading to a final concentration of 1 mg mL^{-1}. The solution was fast stirred using an Ultra-Turrax® (Power 3.5) for 20 min before adding dropwise APTES (0.256 mL) at a ratio of 8:1 (w/w) relative to oxoG. After removing the Ultra-Turrax®, the mixture was then stirred at RT overnight. The mixture is then centrifuged at 5000 rpm, for 15 min at 4 °C. The supernatant was removed, and the precipitate was redispersed in 30 mL of DI water. This purification process is repeated three times. A black dispersion of oxoG-APTES at a concentration of 1.1 mg mL^{-1} was obtained.

2.2. oxoG-APTES-GPTMS. The reaction between oxoG-APTES and GPTMS was conducted using three different conditions: a) in DI water at RT for 24 h; b) in anh. DMF at RT for 24 h; and c) in anh. DMF at 70 °C for 24 h.

2.2.1. oxoG-APTES-GPTMS in H_2O. To a solution of oxoG-APTES, (2 mL, 1.1 mg mL^{-1}), GPTMS (0.015 mL) was added dropwise at a ratio 1:8 (w/w) relative to oxoG-APTES, and the mixture was stirred at RT for 24 h. The solution was then centrifuged at 5000 rpm, for 15 min at 4 °C. The supernatant was removed, and the precipitate was redispersed in DI water (2 mL). This purification process was repeated three times. A black solution of oxoG-APTES-GPTMS in DI water at a concentration of 1.1 mg mL^{-1} was obtained.

2.2.2. oxoG-APTES-GPTMS in anh. DMF at RT. The synthesis of oxoG-APTES-GPTMS in anh. DMF was performed at RT for 24 h. Briefly, 2 mL of previously synthesized oxoG-APTES were filtered on a 0.1 µm PTFE membrane Omnipore (Merck Millipore). Under N_2, the resulting powder was added into a Schlenk and dispersed in 2 mL of anh. DMF. The mixture was fast stirred with a Ultra-Turrax® (Power 3.5) for 20 min followed by the dropwise addition of GPTMS (0.015 mL) at an 8:1 (w/w) ration with respect to oxoG-APTES. The resulting mixture was then stirred at RT for 24 h. The solution is centrifuged at 5000 rpm, for 15 min at 4 °C. The supernatant was removed, and the precipitate was redispersed in DMF (2 mL). The process was repeated three times. A black solution of oxoG-APTES-GPTMS in DMF at a concentration of 1.1 mg mL^{-1} was obtained.

2.2.3. oxoG-APTES-GPTMS in anh. DMF at 70 °C. This reaction was conducted following the same steps of reaction b), but heating the reaction mixture at 70 °C.

2.3. oxoG-APTES-GPTMS-FMBA. To the previously synthesized oxoG-APTES-GPTMS (*i.e.*, anh. DMF at 70 °C) (2 mL, 1.1 mg mL^{-1}), FMBA (6.04 µL) was added dropwise at an 8:1 (w/w) ratio with respect to oxoG-APTES-GPTMS. The dispersion was stirred at 70 °C for 24 h. The solution was then centrifuged at 5000 rpm, for 15 min at 4 °C. The supernatant was removed, and the precipitate was redispersed in DMF (1 mL). The process was repeated three times. A black solution of oxoG-APTES-GPTMS-FMBA in DMF at a concentration of 1 mg mL^{-1} was obtained.

2.4. ^{1}H NMR of GPTMS in DMF-d_7

^{1}H NMR (500 MHz, DMF-d_7, δ): 3.73 (dd, *J* = 11.5, 2.8 Hz, 1H), 3.49 – 3.40 (m, 2H), 3.28 (dd, *J* = 11.5, 6.3 Hz, 1H), 3.12 (ddt, *J* = 6.3, 4.2, 2.7 Hz, 1H), 2.75 (1H, under residual DMF signal) 2.58 (dd, *J* = 5.2, 2.6 Hz, 1H), 1.67 – 1.59 (m, 2H), 0.69 – 0.62 (m, 2H).

2.5. ^{1}H NMR of TES in DMF-d_7

^{1}H NMR (500 MHz, DMF-d_7, δ): 5.28 (s, 1H), 0.95 (t, *J* = 8.0 Hz, 9H), 0.52 (q, *J* = 8.0 Hz, 6H).

2.6. ^{1}H NMR of FMBA in DMF-d_7

^{1}H NMR (500 MHz, DMF-d_7, δ): 7.71 – 7.61 (m, 4H), 3.90 (q, *J* = 0.9 Hz, 2H), 1.96 (s, 2H).

2.7. Phenylmethan-d_2-amine-d_2 (benzylamine-d_4). The synthesis of benzylamine-d_4 was reproduced as described in the literature.[34] Briefly, to a solution of $LiAlD_4$ (100 mg, 2.5 mol L^{-1}) in anhydrous tetrahydrofuran (1 mL) at 0 °C, benzonitrile (51 µL, 0.5 mmol) was added dropwise. The resulting mixture was then stirred at RT for 24 h. D_2O (2 mL) was then added, and the mixture was extracted with $CDCl_3$ (3×5 mL). The combined organic layers were dried over Na_2SO_4 and concentrated under reduced pressure to give phenylmethan-d_2-amine-d_2 as a slightly yellow oil.

^{1}H NMR (500 MHz, DMF-d_7, δ): 7.91 – 7.85 (m, 2H), 7.81 – 7.74 (m, 1H), 7.69 – 7.61 (m, 2H); ^{13}C NMR (126 MHz, DMF-d_7, δ): 134.39, 133.41, 130.66.

2.8. Benzylamine. The same procedure and amounts of reagents used for the synthesis of benzylamine-d_4 was applied with non-deuterated reagents.

^{1}H NMR (500 MHz, DMF-d_7, δ): 7.52 – 7.11 (m, 4H), 3.80 (s, 2H).
^{13}C NMR (126 MHz, DMF-d_7, δ): 140.40, 129.20, 128.16, 127.27.

2.9. Synthesis of TES-GPTMS. In an NMR tube, TES (6.52 µL, 1 equiv) was added to a solution of GPTMS (9.34 µL, 1 equiv) in 0.6 mL of DMF-d_7. The resulting solution was heated at 70 °C for 3 days and analyzed by ^{1}H NMR without purification.

2.10. Synthesis of TES-GTPMS-FMBA. To the previous TES-GPTMS solution in DMF-d_7 (0.6 mL), FMBA (6.04 µL, 1 equiv) was added, and the mixture was heated at 70 °C for 4 days. The solution was then analyzed by ^{1}H NMR without purification.

2.11. Synthesis of TES-GPTMS-benzylamine-d_4. To a solution of TES-GPTMS in DMF-d_7, benzylamine-d_4 (4.29 µL, 1 equiv) was added and the mixture was heated at 70 °C for 4 days. The solution was then analyzed by ^{1}H NMR without purification.

2.12. Synthesis of TES-GPTMS-benzylamine. To a solution of TES-GPTMS in DMF-d_7, benzylamine (4.29 µL, 1 equiv) was added and the mixture was heated at 70 °C for 4 days. The solution was then analyzed by ^{1}H NMR without purification.

Conclusions

By using ^{1}H NMR spectroscopy and simplified reaction models, we unravelled the reactivity of two bifunctional molecules (APTES and GPTMS) on oxo-graphene, rendering possible the elucidation of the structure of the resulting conjugates. This work provides a comprehensive and detailed analysis of the covalent functionalization of oxoG with APTES, GPTMS and FMBA. We demonstrated that APTES reacts with oxoG primarily through its amino group via epoxide ring opening, while leaving the siloxane moiety available for subsequent condensation reactions. GPTMS was shown to react with oxoG-APTES through silanization, and the terminal epoxide of GPTMS remained accessible for further nucleophilic attack. These findings were confirmed using model reactions involving TES-OH and nucleophiles such as FMBA and deuterated benzylamine, providing unambiguous evidence for the reaction pathways.

Moreover, our study highlights the critical influence of the reaction conditions and the choice of solvents when covalently modifying graphene-based materials. Indeed, GPTMS undergoes rapid hydrolysis and self-polymerization in aqueous media, suggesting that it might not react as expected during the silanization reaction.

Overall, this work establishes a robust methodology to verify the covalent functionalization of nanomaterials, especially oxoG or GO, with bi- or multi-functionalities. It also emphasizes the necessity of careful analytical characterizations to accurately interpret the covalent multistep modifications on graphene-based materials. Finally, the insights gained here provide a foundation for the rational design of multifunctional graphene derivatives with controlled surface chemistry.

Author contributions

OS performed all experiments and characterizations, and wrote the first draft; IJ, BM, CC contributed to the characterizations: SE provided graphene; PS, SG, AB supervised the work and provided fundings. All authors discussed the results and contributed to the final version of the manuscript.

Conflicts of interest

There are no conflicts to declare.

Data availability

All data supporting the findings of this study within the article and its supplementary information (ESI) are available from the

corresponding author, upon reasonable request.

Acknowledgements

This work was supported by the Centre National de la Recherche Scientifique (CNRS), by the ANR through the Interdisciplinary Thematic Institute SysChem, through the IdEx Unistra (ANR-10-IDEX-0002) within the program Investissement d'Avenir, the CSC Graduate School (CSC-IGS ANR-17-EURE-0016) within the French Investments for the Future Program, the Foundation Jean-Marie Lehn and the Institut Universitaire de France (IUF). The authors wish to thank M. Maranska for her help in the synthesis of oxoG.

Notes and references

1. A. A. Balandin, S. Ghosh, W. Bao, I. Calizo, D. Teweldebrhan, F. Miao and C. N. Lau, *Nano Lett.*, 2008, **8**, 902–907.
2. P. Zhu, Y. Yan, Y. Zhou, Z. Qi, Y. Li and C.-M. Chen, *ACS Appl. Nano Mater.*, 2024, **7**, 8445–8463.
3. H. Chen, M. B. Müller, K. J. Gilmore, G. G. Wallace and D. Li, *Adv. Mater.*, 2008, **20**, 3557–3561.
4. L. Liao, H. Peng and Z. Liu, *J. Am. Chem. Soc.*, 2014, **136**, 12194–12200.
5. A. H. Castro Neto, F. Guinea, N. M. R. Peres, K. S. Novoselov and A. K. Geim, *Rev. Mod. Phys.*, 2009, **81**, 109–162.
6. D. G. Papageorgiou, I. A. Kinloch and R. J. Young, *Prog. Mater. Sci.*, 2017, **90**, 75–127.
7. L. R. Radovic and B. Bockrath, *J. Am. Chem. Soc.*, 2005, **127**, 5917–5927.
8. S. Qamar, N. Ramzan and W. Aleem, *Synth. Met.*, 2024, **307**, 117697.
9. W. S. Hummers and R. E. Offeman, *J. Am. Chem. Soc.*, 1958, **80**, 1339.
10. S. Zhang, H. Wang, J. Liu and C. Bao, *Mater. Lett.*, 2020, **261**, 127098.
11. S. Guo, S. Garaj, A. Bianco and C. Ménard-Moyon, *Nat. Rev. Phys.*, 2022, **4**, 247–262.
12. D. R. Dreyer, S. Park, C. W. Bielawski and R. S. Ruoff, *Chem. Soc. Rev.*, 2010, **39**, 228–240.
13. W. Yu, L. Sisi, Y. Haiyan and L. Jie, *RSC Adv.*, 2020, **10**, 15328–15345.
14. S. Eigler, *Chem. Eur. J.*, 2016, **22**, 7012–7027.
15. I. A. Vacchi, C. Spinato, J. Raya, A. Bianco and C. Ménard-Moyon, *Nanoscale*, 2016, **8**, 13714–13721.
16. A. Ahmadi, B. Ramezanzadeh and M. Mahdavian, *RSC Adv.*, 2016, **6**, 54102–54112.
17. C. T. P. da Silva, J. P. Monteiro, E. Radovanovic and E. M. Girotto, *Sens. Actuators, B*, 2014, **191**, 152–157.
18. K. Thorshaug, T. Didriksen, I. T. Jensen, P. Almeida Carvalho, J. Yang, M. Grandcolas, A. Ferber, A. M. Booth, Ö. Ağaç, H. Alagöz, N. Erdoğan, A. Kuban and B. D. Belle, *Nanoscale Adv.*, 2024, **6**, 2088–2095.
19. J. Huang, S. Ding, W. Xiao, Y. Peng, S. Deng and N. Zhang, *Catal. Lett.*, 2015, **145**, 1000–1007.
20. M. Li, C. Tang, L. Zhang, B. Shang, S. Zheng and S. Qi, *J. Mater. Sci.: Mater. Electron.*, 2017, **28**, 15694–15700.
21. N. Bouazizi, J. Vieillard, R. Bargougui, N. Couvrat, O. Thoumire, S. Morin, G. Ladam, N. Mofaddel, N. Brun, A. Azzouz and F. Le Derf, *J. Alloys Compd.*, 2019, **771**, 1090–1102.
22. T. Serodre, N. Oliveira, D. Miquita, M. Ferreira, A. Santos, V. Resende and C. Furtado, *J. Braz. Chem. Soc.*, 2019, **30**, 2488–2499.
23. T.-R. Ovari, B. Trufán, G. Katona, G. Szabó and L. M. Muresan, *RSC Adv.*, 2024, **14**, 10826–10841.
24. X. Kong, J. Liu, S. Li and M. Yu, *Corros. Sci.*, 2023, **213**, 110966.
25. J. H. Lee and S. H. Kim, *Sci. Rep.*, 2020, **10**, 19152.
26. X. Pu, H.-B. Zhang, X. Li, C. Gui and Z.-Z. Yu, *RSC Adv.*, 2014, **4**, 15297–15303.
27. S. S. R. Vuppaladadium, T. Agarwal, S. Kulanthaivel, B. Mohanty, C. S. Barik, T. K. Maiti, S. Pal, K. Pal and I. Banerjee, *Mater. Sci. Eng. C*, 2020, **110**, 110647.
28. S. Nezamdoust and D. Seifzadeh, *Prog. Org. Coat.*, 2017, **109**, 97–109.
29. Y. Kim, H. Park and B. Kim, *High Perform. Polym.*, 2015, **27**, 886–897.
30. X. Zhi, Y. Mao, Z. Yu, S. Wen, Y. Li, L. Zhang, T. W. Chan and L. Liu, *Compos. Part A Appl. Sci. Manuf.*, 2015, **76**, 194–202.
31. C.-C. Liu, J.-J. Zhao, R. Zhang, H. Li, B. Chen, L.-L. Zhang and H. Yang, *Am. J. Transl. Res.*, 2017, **9**, 5197–5219.
32. M. G. Gonçalves, V. O. Costa, A. H. G. Martinez, B. M. Régnier, G. C. B. Gomes, A. J. G. Zarbin and E. S. Orth, *Front. Carbon*, 2024, **3**, 1393077.
33. G. Reina, C. Gabellini, M. Maranska, F. Grote, S. M. Chin, L. Jacquemin, F. Berger, P. Posocco, S. Eigler and A. Bianco, *Carbon*, 2022, **195**, 69–79.
34. T. Zhang, X. An, G. Cui, H. Ma, X. He and M. Wang, *J. Org. Chem.*, 2025, **90**, 3322–3333.
35. Y. Qian, C. Zhou and A. Huang, *Carbon*, 2018, **136**, 28–37.
36. M. Hu and B. Mi, *Environ. Sci. Technol.*, 2013, **47**, 3715–3723.
37. M. Zhu, M. Z. Lerum and W. Chen, *Langmuir*, 2012, **28**, 416–423.
38. W.-S. Hung, C.-H. Tsou, M. De Guzman, Q.-F. An, Y.-L. Liu, Y.-M. Zhang, C.-C. Hu, K.-R. Lee and J.-Y. Lai, *Chem. Mater.*, 2014, **26**, 2983–2990.
39. P. Innocenzi, C. Figus, T. Kidchob, M. Valentini, B. Alonso and M. Takahashi, *Dalton Trans.*, 2009, 9146–9154.
40. C. A. Casagrande, L. F. Jochem and W. L. Repette, *Matéria (Rio J.)*, 2020, **25**, e-12811.
41. A. Ganguly, S. Sharma, P. Papakonstantinou and J. Hamilton, *J. Phys. Chem. C*, 2011, **115**, 17009–17019.
42. S. Eigler and A. Hirsch, *Phys. Sci. Rev.*, 2017, **2**, e20160106.
43. S. Eigler, C. Dotzer, F. Hof, W. Bauer and A. Hirsch, *Chem. Eur. J.*, 2013, **19**, 9490–9496.
44. K. M. Aujara, B. W. Chieng, N. A. Ibrahim, N. Zainuddin and C. Thevy Ratnam, *Int. J. Mol. Sci.*, 2019, **20**, 1910.
45. N. I. Khan, S. Halder, N. Talukdar, S. Das and M. S. Goyat, *Mater. Chem. Phys.*, 2021, **258**, 123851.
46. L. Gabrielli, L. Russo, A. Poveda, J. R. Jones, F. Nicotra, J. Jiménez-Barbero and L. Cipolla, *Chem. Eur. J.*, 2013, **19**, 7856–7864.
47. W. Lu, A. T. Tarekegne, Y. Ou, S. Kamiyama and H. Ou, *Sci. Rep.*, 2019, **9**, 16333.

View Article Online
DOI: 10.1039/D6NR01024E

Data availability

All data supporting the findings of this study within the article and its supplementary information (ESI) are available from the corresponding author, upon reasonable request.